Micromechanics Based Stress-Displacement Relationships of Rough Contacts: Numerical Implementation under Combined Normal and Shear Loading

Anil Misra[1] and Shiping Huang[1]

Abstract: The behavior of contact between solid bodies with rough surfaces under combined normal and shear loading remains a problem of interest in many areas of engineering. In this paper, we have utilized a micromechanical methodology to derive an expression of stress-displacement relationship applicable to combined normal and shear loading conditions. The micromechanical methodology considers the mechanics of asperity contacts and the interface roughness in terms of asperity height and asperity contact orientation distribution. A numerical procedure is implemented to evaluate the derived expressions under complex and mixed loading conditions using an incremental approach. We find that the proposed numerical procedure provides accurate results under all kind of loading conditions, although the number of steps to convergence depends upon the initial assumption. The results show that the interface closure behavior is highly nonlinear and does not follow a power-law although a Hertzian model is used for asperity contacts. Numerical results also confirm the experimental observation that rougher interfaces are softer and have higher frictional strength compared to smooth interfaces under shear loading.

1   Introduction

Contact between solid bodies is ubiquitous in nature and contact problems abound across all areas of engineering. The understanding and modeling of stress-displacement behavior of a contact has been one of the most widely researched problems with contributions spanning more than a century. This paper considers the contact of relatively stiff bodies undergoing small normal deformations, such as those found

---

[1] Department of Civil, Environmental and Architectural Engineering, the University of Kansas, KS,U.S.A.

in fractured media, jointed rock masses, masonry structures, granular geomaterials, and in structural and machine assemblies. The pioneering work along these lines was performed by Hertz with regards to contact of perfectly smooth rotund elastic bodies (Johnson 1985). With the advancement in the measurement of surface profiles and contact behavior, it has become clear that all surfaces consist of numerous irregular asperities and the surface roughness has a significant role in determining the mechanical behavior. Accordingly, numerous researchers have investigated the mechanical behavior of contacting surfaces by explicitly modeling the behavior of asperity contacts.

Among the early efforts along these lines, Greenwood and Williams (1966) introduced the statistical approach to describe the roughness of the interface, assuming each asperity had the same radius but different heights. Since then statistical methods have prevailed and a vast amount of literature has been contributed to this field. Whitehouse and Archard (1970) developed the Greenwood and Williamson (G-W) model by accounting for the random radii of curvature of the asperity tips. Nayak (1971, 1973) introduced the techniques of random process theory into the analysis of Gaussian roughness which was subsequently used by Bush, Gibson and Thomas (1975) in rough surface contact. Adler and Firman (1981) proposed a non-Gaussian random surfaces; Yamada, Takeda, Kagami and Naoi (1978a, 1978b) derived his contact model formed by two rough surfaces described by probability density function of the peak height of each asperity; Brown and Scholz (1985, 1986) presented a composite height model for the contact between two random nominally flat elastic surfaces. McCool and co-worker (Mccool 1986; Mccool and Gassel 1981) treated anisotropic rough surfaces with ellipsoidal asperities, however, they found a good agreement with the simpler G-W model and suggested that spherical shape asperity assumption is not only simplifying but also representative of the asperity contact behavior. More recently, Persson and coworkers have developed an alternative theory for contact between solids by considering the real contact area of self-affine surfaces undergoing large deformations (see Persson 2007) and references therein). A preponderance of the above-cited work (Brown and Scholz 1985, 1986; Bush, Gibson and Thomas 1975; Greenwood and Williams 1966; Mccool 1986; Mccool and Gassel 1981; Whitehouse and Archard 1970) was concerned with contact behavior under loading in the normal direction to the nominal orientation of the interface. Under shear loading, sliding of asperity contact becomes significant in determining the overall friction of the interface. The early work related to the modeling of friction of the rough interface was done by Archard (1957). Contact friction and its dependence on interface roughness has been widely recognized and deemed important in a variety of problems as seen from the recent works of Ozaki, Hashiguchi, Okayasu and Chen (2007), Guz, Menshykov, Zozulya and Guz (2007);

Guz and Zozulya (2007), Vignjevic, De Vuyst and Campbell (2006) and many others. Clearly, both contact closure and friction modeling remains an active area and satisfactory models for rough contacts under combined normal and shear loading remain elusive.

To obtain a deeper understanding of contact problems under both normal and shear loading, numerical approach, such as the finite element and the meshfree methods have been utilized recently (see Wriggers 2006, Selvadurai and Yu 2005, Sellgren, Bjorklund and Andersson 2003, Hyun, Pei, Molinari and Robbins 2004, Shankar and Mayuram 2008, Vignjevic, De Vuyst and Campbell 2006, Han, Liu, Rajendran and Atluri 2006 and many others). The foremost limitation of the finite element and meshfree methods remains their computational expense especially when dealing with 3-dimensional contact problems involving numerous asperities. Consequently, methods that utilize statistical descriptions of the interface roughness continue to be attractive. Along these lines, the author has developed a kinematically driven micromechanical methodology for contacting rough surfaces by considering asperity heights and asperity contact orientation distributions (Misra 1997, 1999). In this paper, we have utilized this micromechanical methodology to derive an expression of stress-displacement relationship applicable to combined normal and shear loading conditions. A numerical procedure is implemented to evaluate the derived expressions under complex and mixed loading conditions using the Newton-Raphson method to solve the nonlinear stress-deformation equations in an incremental manner. The present work extends the statistical approach by incorporating (1) a directional distribution function of asperity contact orientations as an additional measure of surface roughness, and (2) an iterative procedure to obtain the asperity contact forces at each load increment recognizing that the asperity contact force distribution is not known a priori.

In the subsequent discussion, we first briefly present our approach for statistical modeling of contact surface and the essence of the kinematically driven micromechanical methodology. We then describe the numerical procedure based upon Newton-Raphson method for evaluating the stress-displacement relationship. Finally we present computed stress-displacement relationships under various boundary conditions used in the laboratory testing performed on contacting solid bodies. We find that the proposed numerical procedure provides accurate results under all kind of loading conditions, although the number of steps to convergence depends upon the initial assumption. The results show that the interface closure behavior is highly nonlinear and does not follow a power-law although a Hertzian model is used for asperity contacts. Numerical results also confirm the experimental observation that rougher interfaces are softer and have higher frictional strength compared to smooth interfaces under shear loading.

2   Statistical Description of Contact Interface

The contacting surface geometry determines the orientations and the number of asperity contacts under a given loading condition. The composite topography defined as the sum of the contacting surface profiles and described via statistics of asperity contact heights, orientations, and curvatures may be utilized for this purpose (Adler and Firman 1981; Misra 1997; Nayak 1971; Yoshioka 1994). In this paper, the statistics of asperity contact heights is described via gamma distributions, asperity contact orientations via spherical harmonic expansions, and asperity curvatures are assumed to be constant for simplicity. It is usual to define the asperity contact height with reference to the highest peak of the composite topography such that, asperity height, r, represents the overlap of the interacting surfaces. The density function for asperity heights, $H(r)$, is given by a gamma distribution (Adler and Firman 1981; Yoshioka and Scholz 1989a, 1989b) expressed as:

$$H(r) = \frac{r^{\alpha} e^{-r/\beta}}{\Gamma(\alpha+1)\beta^{\alpha}} \quad (0 < r < \infty, \ \alpha > -1, \ \beta > 0) \tag{1}$$

where α and β are parameters related to the mean and variance of the asperity heights as follows

$$\begin{aligned} mean: & \quad r_m = (\alpha+1)\beta \\ variance: & \quad r_{\sigma}^2 = (\alpha+1)\beta^2 \end{aligned} \tag{2}$$

Parameter α is unit less while parameter β takes the unit of asperity height. Surfaces that have smaller average asperity height and narrow distributions of asperity heights are considered to be smoother. Fig. 1 gives examples of asperity height distributions for two interfaces that can be described as smooth and rough in comparison with each other. For an interface with N asperities per unit area, $NH(r)\,dr$ denotes that number of asperity contacts in the interval represented by r and $r + dr$. Thus, the total number of asperity contacts, under a given closure, is given by

$$N_r = \int_0^r NH(r)\,dr \tag{3}$$

In order to describe the orientation distribution, we introduce a local Cartesian coordinate system as shown in Fig. 2. The local coordinate system consists of three vectors n, s and t, among which **n** is the vector normal to the asperity contact surface, and **s** and **t** are on the plane tangential to the asperity contact surface. The relationship between the local coordinate system and the global Cartesian system
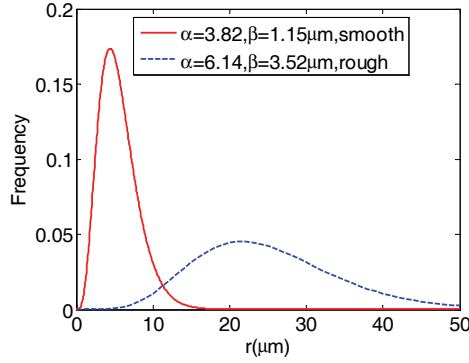
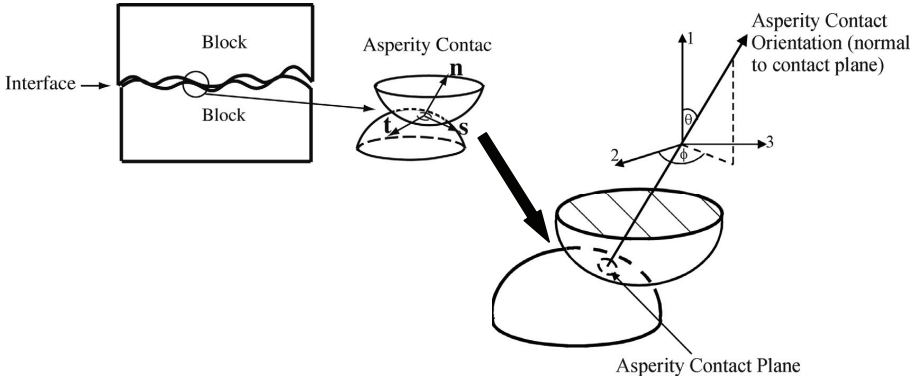Figure 1: Examples of contact height distributions.

Figure 2: Schematic depiction of the micromechanical modeling methodology for rough interfaces.

is given by:

$$n_i = \langle \cos\theta, \quad \sin\theta\cos\phi, \quad \sin\theta\sin\phi \rangle$$
$$s_i = \langle -\sin\theta, \quad \cos\theta\cos\phi, \quad \cos\theta\sin\phi \rangle \qquad (4)$$
$$t_i = \langle 0, \quad -\sin\theta, \quad \cos\phi \rangle$$

The asperity contact orientation is defined by considering the inclination of the asperity contact normal with respect to that of the interface normal direction. As shown in Fig. 2, the orientation of an oblique asperity contact is defined by the azimuthal angle, ϕ, and the meridional angle, θ, measured with respect to a Cartesian coordinate system in which direction 1 is normal to the interface. A 3-dimensional

density function utilizing shifted spherical harmonics expansion in spherical polar coordinates that describes the concentrations of asperity contact orientations was introduced by Misra (1997, 1999). For a rock joint with isotropic distribution of asperity contact orientations, the density function, $\xi(\Omega)$, is defined in the domain: $0 \leq \theta \leq 2\pi/a$, $0 \leq \phi \leq 2\pi$, given by

$$\xi(\Omega) = \frac{a \sin a\theta}{2\pi \sin \theta} \left[1 + \frac{b}{4}(3\cos a\theta + 1) + 3c(\sin a\theta)^2 \cos 2\phi \right]$$

$$\left(0 \leq \theta \leq \tfrac{\pi}{2a}; \quad 0 \leq \phi \leq 2\pi; \quad a \geq 1 \right) \tag{5}$$

where angles ϕ and θ are defined in Fig. 2 Ω represents the solid angle formed by ϕ and θ, and parameters a and b determine the shape of the density function $\xi(\Omega)$. Thus, the product $N_r\xi(\Omega)d\Omega$ denotes the number of asperity contacts NΩ in the interval represented by solid angles Ω and $\Omega+d\Omega$, that is

$$N_\Omega = N_r\xi(\Omega)d\Omega \tag{6}$$

The orientation parameters a and b are related to the mean and variance of asperity contact orientations as follows

$$E[\theta] = \frac{6-b}{6a} \quad \text{and} \quad E\left[(\theta - E[\theta])^2\right] = \frac{36\pi - 108 + 20b - 6b\pi - b^2}{36a^2} \tag{7}$$
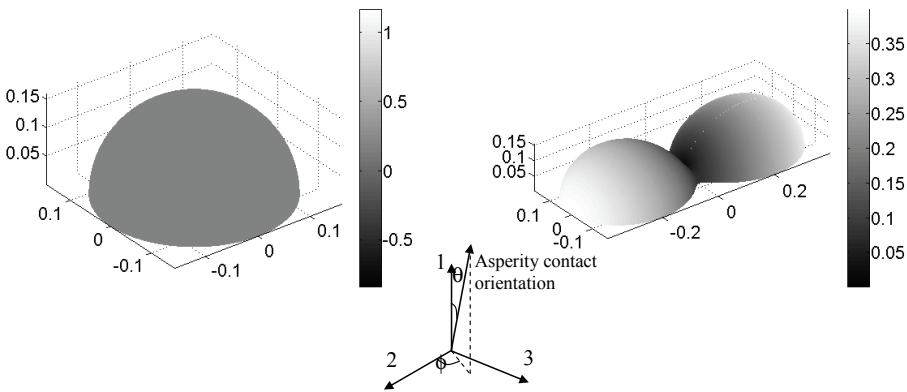

Figure 3: Contact orientation distributions: left frame is for isotropic interface (a=1,b=0,c=0) and right frame is for anisotropic interface (a=1,b=-1,c=1/3). Grayscales indicate the probability density of finding asperity contact in a given orientation defined by the coordinate system.

The density function in Eq.(5) has the ability to model surfaces with varying roughness. As discussed in Misra (1999), more asperity contacts orient in the direction perpendicular to the interface for smooth surfaces than that for rough surfaces. Accordingly, as parameter, a, increases, the contact distribution concentrates towards the direction normal to the interface (along the 1-axis of the global Cartesian coordinate system in Fig. 2). In particular, the density function, $\xi(\Omega)$, behaves like a delta function in the limit $a \to \infty$ and yields an expectation $E[\theta] = 0$, which represents a concentrated contact orientation, normal to a perfectly smooth interface. The parameter, a, describes the extent of the asperity contacts in the meridional direction as well as the mean asperity contact orientation. Fig. 3 show the 3-dimention distribution density for different combination of parameters a, b and c.

3   Micromechanical Stress-Displacement Relationship

In the kinematically driven approach, we assume that the asperity displacement, δ_j, at a given asperity height is the same and directly related to the overall displacement of the interface, Δ_j. The subscripts in this paper follow the established tensor convention unless specified otherwise. Under the kinematic assumption, the asperity displacement in the local coordinate system can be written in terms of the overall interface displacements as follows:

$$
\begin{Bmatrix} \delta_n \\ \delta_s \\ \delta_t \end{Bmatrix} = \begin{bmatrix} n_1 & n_2 & n_3 \\ s_1 & s_2 & s_3 \\ t_1 & t_2 & t_3 \end{bmatrix} \begin{Bmatrix} \Delta_1 - r \\ \Delta_2 \\ \Delta_3 \end{Bmatrix} \tag{8}
$$

Note that we assume the asperities to have spherical shape with the same radius but different heights. Therefore, for a normal interface displacement Δ_1, the displacement of the asperity at height r is $\Delta_1 - r$. This kinematic assumption disregards the nonlocality of asperity contact interactions. The assumption is reasonable for interfaces with relatively large asperity spacing in stiff materials such that the overlap of deformation fields associated with neighboring asperity contacts is minimal and the statistical description of the interface remains unchanged during loading. This assumption has been widely used and appears to be especially useful for describing contacts between metals and stiff geomaterials, such as rock joints (Brown and Scholz 1986; Greenwood and Williams 1966). In some cases, however, the asperities may undergo damage. The consequent change in the interface geometry has to be appropriately modeled (Misra 2002).

In local coordinate system, considering the Hertz-Mindlin contact theory of perfectly smooth elastic interfaces as well as other theories of smooth elastic-plastic interfaces(Johnson 1985), it is reasonable to assume that normal asperity stiffness K_n

depends on the normal asperity displacement δ_n according to the following power law:

$$K_n = \lambda K \delta_n^\eta \tag{9}$$

Where δ_n is the magnitude of normal compression at the asperity contact, and K, λ and η are constants. The asperity stiffness, K_n given by Eq.(9),becomes identical with the Hertz stiffness for contact of perfectly smooth elastic spheres when

$$\left[\lambda = \frac{2-v}{2(1-v)}; \quad \eta = \frac{1}{2}; \quad K = \frac{8G\sqrt{R}}{3(2-v)}\right] \tag{10}$$

where G is the shear modulus, v is Poisson's ratio and R is asperity radius of curvature. It is noteworthy that the exponent η can vary from 0 for perfectly plastic to $1/2$ for perfectly elastic behavior at contact of perfectly smooth spherical asperities (Johnson 1985). Since this paper focuses on monotonic loading of interfaces, we consider the case of constant normal asperity force and monotonically increasing asperity shear force. Mindlin and Deresiewicz (1953) have derived the following asperity force-displacement relationship for this loading condition, considering partial slip at contact edge with increasing contact shear displacement:

$$f_{st} = \mu K_n \delta_n \left[1 - (1 - \frac{\delta_{st}}{\lambda \mu \delta_n})^{\frac{3}{2}}\right] \tag{11}$$

Where f_{st} is the asperity shear force and δ_{st} is the asperity shear displacement given by,

$$\delta_{st} = \sqrt{\delta_s^2 + \delta_t^2} \tag{12}$$

Thus, in s and t direction, we have the following force displacement relationship:

$$f_s = f_{st} \frac{\delta_s}{\delta_{st}} = \mu K_n \frac{\delta_n}{\delta_{st}} \left[1 - (1 - \frac{\delta_{st}}{\lambda \mu \delta_n})^{\frac{3}{2}}\right] \delta_s = K_s \delta_s \tag{13}$$

$$f_t = f_{st} \frac{\delta_t}{\delta_{st}} = \mu K_n \frac{\delta_n}{\delta_{st}} \left[1 - (1 - \frac{\delta_{st}}{\lambda \mu \delta_n})^{\frac{3}{2}}\right] \delta_t = K_t \delta_t \tag{14}$$

where Ks and Kt are stiffness in s and t directions, respectively. We note Eqs. (13) and (14) are valid when $\lambda \mu \delta_n > \delta_{st}$. When this condition is violated, sliding occurs at the contact per the Amonton–Coulomb's friction law. In this case Eqs. (13) and (14) can be rewritten as:

$$f_s = \mu K_n \frac{\delta_n}{\delta_{st}} \delta_s = K_s \delta_s \tag{15}$$

$$f_t = \mu K_n \frac{\delta_n}{\delta_{st}} \delta_t = K_t \delta_t \tag{16}$$

Thus, for a single asperity contact the force-displacement can be written in the following matrix form in the local coordinate system:

$$\begin{Bmatrix} f_n \\ f_s \\ f_t \end{Bmatrix} = \begin{bmatrix} K_n & 0 & 0 \\ 0 & K_s & 0 \\ 0 & 0 & K_t \end{bmatrix} \begin{Bmatrix} \delta_n \\ \delta_s \\ \delta_t \end{Bmatrix} \tag{17}$$

Or in the global coordinate system, the asperity contact forces, f_i, and displacements, δ_j, are related as follows:

$$\begin{Bmatrix} f_1 \\ f_2 \\ f_3 \end{Bmatrix} = \begin{bmatrix} K_{11} & K_{12} & K_{13} \\ K_{12} & K_{22} & K_{23} \\ K_{13} & K_{23} & K_{33} \end{bmatrix} \begin{Bmatrix} \Delta_1 - r \\ \Delta_2 \\ \Delta_3 \end{Bmatrix} \quad or \quad f_i = K_{ij}(\Delta_j - \delta_{1j}r) \tag{18}$$

Where the asperity contact stiffnesses, K_{ij}, given by:

$$K_{ij} = K_n n_i n_j + K_s s_i s_j + K_t t_i t_j \tag{19}$$

where K_n, K_s and K_t denote asperity stiffness along the n, s and t direction of the asperity contact.

At a rough interface, numerous asperity contacts of varying height overlap and orientations occur under a given loading condition. These asperity contacts can be classified into three groups: (1) those in contact but without sliding, (2) those in contact but with sliding, and (3) those not in contact. The overall interface stress can be obtained as the sum of the asperity contact forces contributed by groups (1) and (2). Utilizing the orientation distribution and height distribution introduced in section 2, we obtain the following expression for the overall interface stress:

$$F_i = N(\int_{r^e} \int_{\Omega^e} f_i^e \xi(\Omega) d\Omega H(r) dr + \int_{r^p} \int_{\Omega^p} f_i^p \xi(\Omega) d\Omega H(r) dr \tag{20}$$

Where the superscript e denotes the domain and forces of asperity contacts that are not sliding, and the superscript p denotes the domain and forces of asperity contacts experiencing sliding.

4 Numerical implementation for nonlinear force-displacement relationship

Based on the expression derived above, if the overall interface displacements are known, the overall interface stresses can be calculated directly from Eq. (20). However, the loading conditions utilized during laboratory testing of interfaces or for

computations involving fractured bodies are in many cases specified either in terms of stresses or a mix of stresses and displacement. If the stress loading conditions or mixed loading conditions are given, we have to solve the nonlinear equation system given by Eq. (20) to obtain the corresponding displacements. In this paper, we utilize the Newton-Raphson method to solve this set of nonlinear equations. For further discussion, Eq. (20) is rewritten as

$$R_i(\Delta_i) \equiv N(\int_{r^e} \int_{\Omega^e} f_i^e \xi(\Omega) d\Omega H(r) dr + \int_{r^p} \int_{\Omega^p} f_i^p \xi(\Omega) d\Omega H(r) dr) - F_i^E = 0 \quad (21)$$

where $R_i(\Delta_i)$ is the residual vector, F_i^E is understood as the external force vector. We expand the residual $R_i(\Delta_i)$ in Taylor's series with respect to displacement vector Δ_i at $(n-1)^{th}$ iteration to obtain:

$$R_j(\Delta_i) = R_j(\Delta_i)^{n-1} + \left(\frac{\partial R_j}{\partial \Delta_i}\right)^{n-1} d\Delta_i + \ldots \quad (22)$$

where we omit the terms of order 2 and higher. Now, using Eq. (22) we get

$$(T_{ji})^{n-1} d\Delta_i = -R_j(\Delta_i)^{n-1} \quad (23)$$

where T_{ji} is recognized as the tangent stiffness tensor given as,

$$(T_{ji})^{n-1} = \left(\frac{\partial R_j}{\partial \Delta_i}\right)^{n-1} \quad (24)$$

We can thus obtain the increment of displacement, $d\Delta_i$, corresponding to the residual at the $(n-1)^{th}$ iteration as

$$d\Delta_i = \frac{-R_j(\Delta_i)^{n-1}}{(T_{ji})^{n-1}} \quad (25)$$

and, subsequently, update the interface displacement in the usual manner

$$(\Delta_i)^n = (\Delta_i)^{n-1} + d\Delta_i \quad (26)$$

The above numerical scheme has been implemented as follows:

Step 1: Discretize the integration domain in Eq. (20) into sufficient points representing asperity contact heights and orientations so as to obtain a converged solution. For our computations we have used $\Delta r = 0.01 r_{90}$, where $r_{90} =$ is the 90th percentile of asperity height for $r-$discretization, and grid of 20x40 for θ and $\phi-$discretization. The integration is performed using Simpson's rule.

Step 2: Use the $(n-1)^{th}$ iteration displacement $(\Delta_i)^{n-1}$ to determine sliding condition of each contact point and sum all of the forces of contacts points to obtain the overall force, $(F_i)^{n-1}$, using discretized Eq. (20).

Step 3: Use a small interface displacement increment, $\partial \Delta_i$, typically taken as $0.01 r_{90}$, to compute the corresponding increment of interface force, ∂F_j, following step 2 and evaluate tangential stiffness $(T_{ji})^{n-1} = \left(\frac{\partial F_j}{\partial \Delta_i} \right)^{n-1}$.

Step 4: Calculate the residual force $R_j^{n-1} = F_j^E - (F_j)^{n-1}$, and use Eq. (25) to find the interface displacement increment, $d\Delta_i$. Update the interface displacement $(\Delta_i)^n$ and check for convergence.

5   Results and Discussion

We demonstrate the applicability of the derived overall stress-displacement relationship and its numerical implementation under a variety of loading conditions. The interface properties used for our example computations are tabulated in Tab. 1. These parameters are for illustrative purposes and are loosely based upon observations of lab tests on stiff rock, ceramic and metal samples. Example computations are performed for (1) normal (1-d) loading under specified interface normal stress, (2) combined normal and shear (2-d) loading under specified normal and shear stresses as well as specified normal stress and shear displacement. In particular, these computations illustrate (1) the importance of asperity contact orientations as an additional roughness parameter that is usually disregarded in other treatments of rough contacts in the literature (Zavarise and Paggi 2008), and (2) the coupling between the normal and shear behavior of the interface even though no such coupling is assumed at the asperity contact.

Table 1: Interface property.

asperity number	asperity friction	plasticity parameter	orientation distribution
N=1000 /mm^2	μ=1	η =1/2	a=1,b=0,c=0
Radius	shear modulus	Poisson's ratio	height distribution
R=200 μm	G=80 GPa	ν=0.3	α=6.14, β=3.52 μm

5.1   Normal loading (1-d)

To evaluate our procedure under stress-controlled normal loading conditions, the interface stress was specified as F_1 = 140 MPa, $F_2 = F_3 = 0$. For our computation we took an initial value of normal displacement $\Delta_1^0 = 9\mu$m at first iteration. The results

of the subsequent iterations and convergence are shown in Tab. 2. After 7 itera-
tions, the unbalanced stress is reduced to <1% of the specified normal stress. As
seen from Tab. 2, convergence would be achieved in lesser number of iterations if
the initial assumption was closer to the result. Typically for the first loading incre-
ment, a close initial assumption is not possible. However, for subsequent loading
increment we use the previous increment result as the initial assumption and the
convergence steps can be significantly reduced. Based upon this incremental pro-
cedure we can obtain the complete stress-displacement curve under normal loading
as shown in Fig. 4. We note that the calculated normal stress-displacement behav-
ior does not follow a power-law behavior with the usual Hertzian exponent of 3/2.
Instead, the behavior is highly nonlinear as shown by the nonlinear curve in the
log-log plot in Fig. 4b. This nonlinearity depends upon the initial closure, asperity
contact friction angle and the asperity height distribution. A detailed study of the
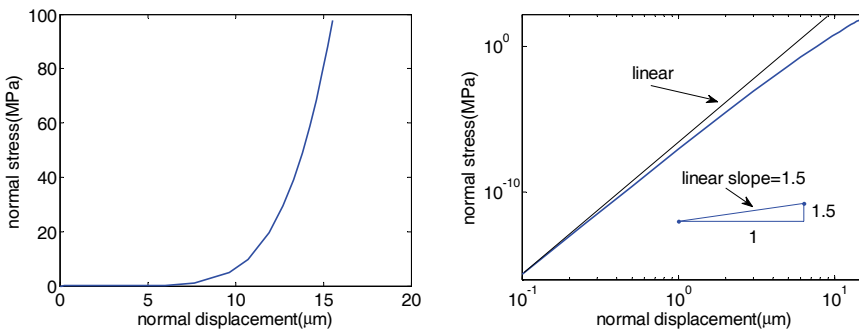closure behavior non-linearity will be described in a future publication.

Figure 4: (a) Normal stress-displacement curve (b) Normal stress-displacement
curve (logarithm plot)

Table 2: Convergence for normal loading.

Iteration, n	0	1	2	3	4	5	6	7
$(\Delta_1)^{n-1} \mu$m	9.00	64.99	37.76	26.91	21.24	18.10	16.75	16.48
R_1^{n-1} MPa	137.0	-27497.0	-5823.0	-1483.0	-400.0	-96.0	-14.0	-0.8

5.2 *Combined normal and shear loading (2-d)*

We consider two cases of combined normal and shear (2-d) loading: case 1 – under
specified normal and shear stresses (stress-loading), and case 2 – under specified

normal stress and shear displacement (mixed-loading). For case 1, the interface stress was specified as: $F_1 = 300$ (MPa), $F_2 = 400$ (MPa), $F_3 = 0$. For our computation we arbitrarily took an initial value of normal displacement $\Delta_1^0 = 30\mu$m, and shear displacement $\Delta_2^0 = 15\mu$m at first iteration, respectively. In this case we have two unknown displacements and the results of the subsequent iterations and convergence are shown in Tab. 3. After 5 iterations, the unbalanced stress is reduced to <1% of the specified stresses.

Table 3: Convergence for 2-d stress loading condition.

Iteration, n	0	1	2	3	4	5
$(\Delta_1)^{n-1}\mu$m	30	23.29	19.86	18.56	18.36	18.35
$(\Delta_2)^{n-1}\mu$m	15	8.99	7.06	6.71	6.76	6.76
R_1^{n-1} MPa	-2710.5	-683.0	-1485.0	-175.0	-5.0	0.0
R_2^{n-1} MPa	-3552.4	-793.4	-1528.0	-129.0	-3.0	-3.0

For case 2, the loading was specified as: $F_1 = 140$ (MPa), $F_3 = 0$, and $\Delta_2 = 5\mu$m. The initial value of the normal displacement Δ_1^0 was taken as 30μm at the first iteration. In this case we have an unknown displacement and an unknown stress. The results of the subsequent iterations and convergence are shown in Tab. 4. After 5 iterations, the unbalanced stress is reduced to <1% of the specified stresses and the shear stress converges to <2% of the previous iteration. We have obtained similar results for 3-dimensional stress- and mixed-loading conditions.

Table 4: Convergence for 2-d mixed loading condition.

Iteration, n	0	1	2	3	4	5
$(\Delta_1)^{n-1}\mu$m	30	22.80	18.78	16.78	16.20	16.15
$(F_2)^{n-1}$ MPa	1151.3	559.9	292.1	191.1	167.9	164.6
R_1^{n-1} MPa	-2485.4	-668.2	-172.1	-32.7	-2.7	0.01

5.3 Qualitative Comparison of Model Prediction with Measurements

Finally, we have utilized the numerical implementation to study the effect of interface roughness upon the friction behavior by applying a constant normal stress, F_1, while monotonically increasing the shear stress, F_2. In the example computation, we have considered (1) the roughness variation due to asperity contact orientations, since the orientation distribution has a critical effect upon the interfacial frictional strength, (2) the roughness variation due to asperity heights, and (3) the effect of

interface normal stress. The result of the friction example is given in Figs. 5a, 5b and 6a, as a plot of shear resistance defined as the ratio of shear to normal stress, F_2/F_1, versus the shear displacement Δ_2. In Fig. 5a, two interfaces with different values of asperity contact orientation parameter, *a*, and same asperity height distributions are considered. The rough interface is represented by asperity contact orientation parameter $a=3$ for the mean asperity inclination of 19.1^o, while the smooth interface is represented by asperity contact orientation parameter $a=10$ for the mean asperity inclination of 5.7^o. Similarly, in Fig. 5b, two interfaces with different asperity height distributions and the same asperity contact orientation parameter are considered. In this case, the rough interface is represented by asperity height distribution parameters $\alpha=6.14$ and $\beta=3.52\mu$m, while the smooth interface by $\alpha=3.82$ and $\beta=1.15\mu$m.
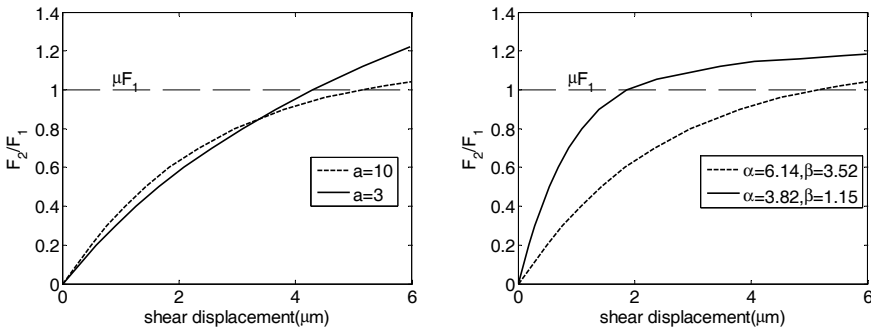

Figure 5: (a) Shear resistance-displacement curves under constant normal stress for a rough (a=3) and a smooth (a=10) interface with same asperity height distributions. (b) Shear resistance-displacement curves under constant normal stress for interfaces with different asperity height distributions and asperity orientation parameter $a=10$.

The difference between the two curves in Figs. 5a and 5b may be considered in two distinct regions of shear displacements; one under small displacements, and the second at large displacement. In the small shear displacement regime, we observe that rough interfaces are less stiff compared to the smooth interfaces. Measurements performed on interfaces of same materials but different roughness (Biegel, Wang, Scholz, Boitnott and Yoshioka 1992; Yoshioka and Scholz 1989) confirm that smoother interfaces are stiffer. The stiffer response of smooth interface can be attributed to the concentration of asperity contact orientation distribution toward the direction normal to the interface or a larger real area of contact. Under
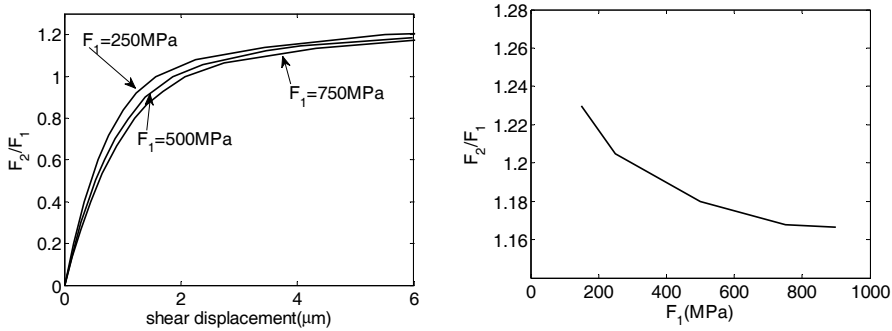
Figure 6: (a) Shear resistance-displacement curves under different constant normal stresses for a relatively smooth interface (α=3.82; β=1.15 and a=10). (b) Interface sliding resistance as a function of normal stress for a relatively smooth interface (α=3.82; β=1.15 and a=10).

small shear displacements, the effect of applied normal stress is dominant. Therefore, interfaces with larger number of asperity contact in the direction normal to the interface or with a larger real contact area tend to be stiffer. At the large shear displacement regime, the effect of different roughness measures (asperity orientation and heights) on the interface behavior is different. We observe in Fig. 5a that the curves crossover and the rough interfaces are found to have a higher shear resistance, and eventually, a higher frictional strength compared to smooth interfaces. As the shear loading is increased, the larger proportion of asperity contacts inclined close to the direction normal to the interface for smooth interface begin to slide at shear resistance close to the asperity friction coefficient. In fact, we can observe from Fig. 5a, that the smooth interface (a=10), will reach a frictional strength only slightly greater than the asperity friction coefficient of 1. In contrast, the curves in Fig. 5b do not crossover and show a tendency to converge to similar shear strength. This result is not unexpected since the asperity contact orientations for these two interfaces are identical. The shear resistance given by the ratio F_2/F_1 tends to the asperity friction coefficient, μ, as the orientation parameter, $a \rightarrow \infty$ representing a perfectly smooth interface irrespective of the height distributions. We note that the asperity contact orientations and asperity heights are correlated; consequently for a real interface the parameters for both the roughness measure should change simultaneously. The example presented here demonstrates the significant role asperity contact orientations play in the determination of the overall shear stress-displacement behavior and, particularly, the shear strength behavior of interfaces. In Fig. 6a and 6b, we illustrate the effect of interface normal on the

shear resistance- displacement behavior. As expected the shear stress close to interface sliding increases with normal stress, however, this increase is nonlinear as shown by the plot of shear resistance versus normal stress in Fig. 6b. We find that the shear resistance decreases (or the effective friction coefficient) decreases with normal stress which is in agreement with experimental studies on interfaces between rock blocks (Jing, Nordlund and Stephansson 1992).

6   Concluding Remarks

Methods that utilize statistical descriptions of the interface roughness continue to be attractive for modeling rough contact behavior. Along this approach, the author has previously presented a micromechanical methodology for contacting rough surfaces by considering asperity heights and asperity contact orientation distributions (Misra 1997, 1999). The applicability of the methodology was widely described; however, the derived approach was not amenable to implementation within larger-scale models that include rough interfaces, such as simulation of jointed rock medium. In this paper, we have utilized this micromechanical methodology to derive an expression of stress-displacement relationship applicable to combined normal and shear loading conditions using an incremental numerical approach. This numerical procedure was implemented to evaluate the derived expressions under complex and mixed loading conditions.

The numerical procedure provides accurate results, although the number of steps to convergence depends upon the initial assumption. The calculated normal stress-displacement behavior is found to be highly nonlinear and does not follow a power-law behavior with the usual Hertzian exponent of 3/2. The calculated shear behavior is found to have a complex dependence upon interface roughness. These results confirm the experimental observation that rougher interfaces are softer and have higher frictional strength compared to smooth interfaces under shear loading. The current model has been described for monotonic loading cases. Modeling of interface behavior under cyclic loading has added complexity arising from several sources, including: (1) asperity behavior under oscillating normal and shear force, (2) evolution of interface structure as asperity contact undergo damage and wear, and (3) numerical implementation. Investigation of cyclic behavior utilizing the approach developed in this paper will be a subject of our future work.

References

Adler, R. J., D. Firman (1981). A Non-Gaussian Model for Random Surfaces. *Philosophical Transactions of the Royal Society of London Series a-Mathematical Physical and Engineering Sciences,* vol. 303 pp 433-462.

Archard, J. F. (1957). Elastic Deformation and the Laws of Friction. *Proceedings of the Royal Society of London Series a-Mathematical and Physical Sciences,* vol. 243 pp 190-205.

Biegel, R. L., W. Wang, C. H. Scholz, G. N. Boitnott, N. Yoshioka (1992). Micromechanics of rock friction, 1, Effects of surface roughness of initial friction and slip hardening in Westerly Granite. *Journal of Geophysical Research-Solid Earth,* vol. 97 pp 8951-8964.

Brown, S. R., C. H. Scholz (1985). Closure of Random Elastic Surfaces in Contact. *Journal of Geophysical Research-Solid Earth and Planets,* vol. 90 pp 5531-5545.

Brown, S. R., C. H. Scholz (1986). Closure of Rock Joints. *Journal of Geophysical Research-Solid Earth and Planets,* vol. 91 pp 4939-4948.

Bush, A. W., R. D. Gibson, T. R. Thomas (1975). Elastic Contact of a Rough Surface. *Wear,* vol. 35 pp 87-111.

Greenwood, J. A., J. B. Williams (1966). Contact of Nominally Flat Surfaces. *Proceedings of the Royal Society of London Series a-Mathematical and Physical Sciences,* vol. 295 pp 300-&.

Guz, A. N., O. V. Menshykov, V. V. Zozulya, I. A. Guz (2007). Contact problem for the flat elliptical crack under normally incident shear wave. *CMES: Computer Modeling in Engineering & Sciences,* vol. 17 pp 205-214.

Guz, A. N., V. V. Zozulya (2007). Investigation of the effect of frictional contact in III-mode crack under action of the SH-Wave harmonic load. *CMES: Computer Modeling in Engineering & Sciences,* vol. 22 pp 119-128.

Han, Z. D., H. T. Liu, A. M. Rajendran, S. N. Atluri (2006). The applications of meshless local Petrov-Galerkin (MLPG) approaches in high-speed impact, penetration and perforation problems. *CMES: Computer Modeling in Engineering & Sciences,* vol. 14 pp 119-128.

Hyun, S., L. Pei, J. F. Molinari, M. O. Robbins (2004). Finite-element analysis of contact between elastic self-affine surfaces. *Physical Review E,* vol. 70 pp -.

Jing, L., E. Nordlund and O. Stephansson (1992). An experimental study on the anisotropy and stress-dependency of the strength and deformability of rock joints. *International Journal of Rock Mechanics Mining Sciences and Geomechanics Abstracts,* vol. 29 pp 535-542.

Johnson, K. L. (1985). Contact mechanics. Cambridge, Cambridge University Press.

Mccool, J. I. (1986). Comparison of Models for the Contact of Rough Surfaces. *Wear,* vol. 107 pp 37-60.

Mccool, J. I., S. S. Gassel (1981). the contact of two surfaces having anisotropic roughness geometry. New York, American Society of Lubrication Engineers.

Mindlin, R. D., H. Deresiewicz (1953). Elastic Spheres in Contact under Varying Oblique Forces. *Journal of Applied Mechanics-Transactions of the Asme,* vol. 20 pp 327-344.

Misra, A. (1997). Mechanistic model for contact between rough surfaces. *Journal of Engineering Mechanics-Asce,* vol. 123 pp 475-484.

Misra, A. (1999). Micromechanical model for anisotropic rock joints. *Journal of Geophysical Research-Solid Earth,* vol. 104 pp 23175-23187.

Misra, A. (2002). Effect of asperity damage on shear behavior of single fracture. *Engineering Fracture Mechanics,* vol. 69 pp 1997-2014.

Nayak, P. R. (1971). Random Process Model of Rough Surfaces. *Journal of Lubrication Technology,* vol. 93 pp 398-&.

Nayak, P. R. (1973). Random Process Model of Rough Surfaces in Plastic Contact. *Wear,* vol. 26 pp 305-333.

Ozaki, S., K. Hashiguchi, T. Okayasu, D. H. Chen (2007). Finite element analysis of particle assembly-water coupled frictional contact problem. *CMES: Computer Modeling in Engineering & Sciences,* vol. 18 pp 101-119.

Persson, B. N. J. (2007). Relation between Interfacial Separation and Load: A General Theory of Contact Mechanics. *Physical Review Letters,* vol. 99 pp 125502.

Sellgren, U., S. Bjorklund and S.,ersson (2003). A finite element-based model of normal contact between rough surfaces. *Wear,* vol. 254 pp 1180-1188.

Selvadurai, A. P. S., Q. Yu (2005). Mechanics of discontinuity in a geomaterial. *Computers and Geotechnics,* vol. 32 pp 92-106.

Shankar, S., M. M. Mayuram (2008). A finite element based study on the elastic-plastic transition behavior in a hemisphere in contact with a rigid flat. *Journal of Tribology-Transactions of the Asme,* vol. 130 pp -.

Vignjevic, R., T. De Vuyst and J. C. Campbell (2006). A frictionless contact algorithm for meshless methods. *CMES: Computer Modeling in Engineering & Sciences,* vol. 13 pp 35-47.

Whitehouse, D. J., J. F. Archard (1970). Properties of Random Surfaces of Significance in Their Contact. *Proceedings of the Royal Society of London Series a-Mathematical and Physical Sciences,* vol. 316 pp 97-&.

Wriggers, P. (2006). Computational contact mechanics. Berlin ; New York, Springer.

Yamada, K., N. Takeda, J. Kagami and T. Naoi (1978a). Mechanisms of Elastic

Contact and Friction between Rough Surfaces. *Wear,* vol. 48 pp 15-34.

Yamada, K., N. Takeda, J. Kagami and T. Naoi (1978b). Surface Density of Asperities and Real Distribution of Asperity Heights on Rubbed Surfaces. *Wear,* vol. 47 pp 5-20.

Yoshioka, N. (1994). Elastic Behavior of Contacting Surfaces under Normal Loads - a Computer-Simulation Using 3-Dimensional Surface Topographies. *Journal of Geophysical Research-Solid Earth,* vol. 99 pp 15549-15560.

Yoshioka, N., C. H. Scholz (1989a). Elastic Properties of Contacting Surfaces under Normal and Shear Loads .1. Theory. *Journal of Geophysical Research-Solid Earth and Planets,* vol. 94 pp 17681-17690.

Yoshioka, N., C. H. Scholz (1989b). Elastic Properties of Contacting Surfaces under Normal and Shear Loads .2. Comparison of Theory with Experiment. *Journal of Geophysical Research-Solid Earth and Planets,* vol. 94 pp 17691-17700.

Zavarise, G., M. Paggi (2008). Reliability of Micromechanical Contact Models: a Still Open Issue. In: P. Wriggers and T. A. Laursen (ed) *CISM International Centre for Mechanical Sciences, 498*, CISM, Udine, Vienna.